Optical force density in waveguides with broken symmetry

Farhan I. Zahin, Tasin Intisar, Li-Fan Yang, and Kevin J. Webb*
Purdue University, West Lafayette, Indiana 47907, USA

(Received 7 October 2025; accepted 19 March 2026; published 23 April 2026)

We investigate the optical force and torque density in relation to the symmetry of dielectric waveguides and reveal a net transverse bulk force associated with eigenmode asymmetry. An estimate of this force under readily realizable conditions indicates that the effect is testable with commonly available equipment. Upon experimental verification, force regulation based on asymmetry could provide a foundation for the optomechanical control of waveguide systems, thereby impacting various optical device technologies, including switches, couplers, and isolators, which would be useful in integrated optical systems.

DOI: 10.1103/p47v-wpf9

I. INTRODUCTION

Symmetry is a foundational principle in the physical and mathematical sciences, serving as a powerful tool for simplifying analyses and predicting system behavior. In periodic systems, such as electronic crystals, photonic crystals, and phononic crystals, periodicity or translational symmetry enables the use of methods like Bloch's theorem, drastically reducing problem complexity. However, when symmetry is broken—as is the case with randomly distributed scatterers [1], in random walks [2], or for aperiodic structures [3,4]—the constraints imposed by symmetry are lifted. This increases the degrees of freedom available for fields, enabling richer behavior. Separately, the concept of parity-time (PT) symmetry has been studied in relation to non-Hermitian quantum mechanics, invariance for simultaneous parity inversion (inversion with respect to a spatial coordinate), and time-reversal operations [5]. Later, PT symmetry in optics considered balanced gain and loss [6,7]. In symmetric waveguide structures, such as those with rectangular or circular cross sections, the eigenmodes inherit the symmetry of the geometry, leading to well-defined even and odd mode patterns. The field solutions in certain waveguide configurations are also periodic due to the geometry, such as in conducting-wall rectangular waveguides (with a periodicity twice the physical dimension) or in the angular dependence of circular waveguides exhibiting axial rotational symmetry. Such symmetry precludes a transverse force stemming from the spatial distribution of the electromagnetic force density in the material composing the waveguide. As we present here, breaking structural symmetry in the cross-section of an optical dielectric waveguide influences the fields and hence the optical force density in a manner that could lead to a net transverse force. This results in a testable concept and potential application spaces.

The study of optical forces builds on more than a century of research into the mechanical action of light. Since the first experimental demonstrations of radiation pressure by Lebedew [8] and by Nichols and Hull [9], the interaction of light and matter has been the subject of extensive theoretical [10–14] and experimental [15–17] investigation. Ashkin's landmark invention of optical tweezers [18] opened new frontiers in microscale manipulation, particularly in biophotonics and cell biology [19,20]. Optical forces have since been harnessed for optomechanical cooling [21], quantum state control [22], and precision metrology [23], as well as for manipulating microstructures in integrated photonic circuits [24–27]. Prior work has examined attractive and repulsive forces between multiple waveguides [28], resonators [29], and between waveguides and substrates [30]. For two parallel waveguides in close proximity, the coupled modes exhibit even or odd symmetries, based on which an attractive or repulsive optical force emerges [31].

The optical force density in a symmetric dielectric waveguide has a symmetry that precludes a net transverse force. In this work, we investigate how breaking structural symmetry modifies optical forces in guided-wave regimes. First, we relate the symmetry properties of waveguide eigenmodes with those of the resulting force density. Subsequently, using numerical simulations, we show that a lossless dielectric waveguide with an asymmetric cross-section can experience a significant transverse optical force during guided-mode propagation, arising from an imbalance in the force density. We estimate that such forces could produce measurable structural deformation, with potential use in integrated optomechanical switching. We further analyze the spatial distribution of torque, providing deeper insight into the expected motion of the structure. These simulation results reveal unanticipated force behaviors in systems with broken symmetry and motivate experiments that may lead to deeper understanding of the spatially distributed electromagnetic force density.

II. OPTICAL FORCE DENSITY THEORY

The fundamental way to model the optical force exerted on a material is to consider the time-dependent electromagnetic force density at each point in space. It is the force density

*Contact author: webb@purdue.edu

exerted at each point that ultimately dictates how a material will move and deform when illuminated. To calculate the force density at each point in space as a function of time, we utilize the work of Einstein and Laub [32]. This formulation can be developed from Maxwell's equations using homogenized constitutive parameters [13,33] and has been considered by us and others (in various forms) in relation to physical and experimental attributes (see, for example, [12,14,17,34–39]). The resulting force density is given by

$$\mathbf{f} = \frac{\partial \mathbf{P}}{\partial t} \times \mu_0 \mathbf{H} - \frac{\partial \mu_0 \mathbf{M}}{\partial t} \times \epsilon_0 \mathbf{E} + \rho \mathbf{E} + \mathbf{J} \times \mu_0 \mathbf{H} + (\mathbf{P} \cdot \nabla)\mathbf{E} + \mu_0 (\mathbf{M} \cdot \nabla)\mathbf{H}, \tag{1}$$

where $\mathbf{P}$ is the polarization, $\mathbf{H}$ is the magnetic field, $\mathbf{M}$ is the magnetization, $\mathbf{E}$ is the electric field, $\mathbf{J}$ is the electric current density, ρ is the electric charge density, ϵ_0 is the permittivity of free space, and μ_0 is the permeability of free space. The derivation of (1), starting from separated material response and source terms in Maxwell's equations, enforces the zero sum of the electromagnetic and kinetic force density at each point in space and time instant [33]. This yields

$$\mathbf{f} = -\left(\nabla \cdot \mathbf{T}_{\mathrm{EL}} + \frac{\partial \mathbf{g}}{\partial t}\right), \tag{2}$$

where $\mathbf{g}$ is the Abraham form of the electromagnetic momentum density used in the development and is given by

$$\mathbf{g} = \frac{1}{c^2} \mathbf{E} \times \mathbf{H}, \tag{3}$$

with c the speed of light in vacuum, and $\mathbf{T}_{\mathrm{EL}}$ the so-called Einstein-Laub stress tensor [32,33], utilized and written as

$$\mathbf{T}_{\mathrm{EL}} = \tfrac{1}{2}(\epsilon_0 \mathbf{E} \cdot \mathbf{E} + \mu_0 \mathbf{H} \cdot \mathbf{H})\mathbf{I} - \mathbf{DE} - \mathbf{BH}, \tag{4}$$

with $\mathbf{I}$ the identity matrix, $\mathbf{D}$ the electric flux density, and $\mathbf{B}$ the magnetic flux density. For this work, we assume nonmagnetic and source-free material ($\rho = 0$, $\mathbf{J} = 0$ and $\mathbf{M} = 0$), simplifying (1) to

$$\mathbf{f} = \frac{\partial \mathbf{P}}{\partial t} \times \mu_0 \mathbf{H} + (\mathbf{P} \cdot \nabla)\mathbf{E}. \tag{5}$$

The mathematical description in (5) holds for stationary media. Thus, in a sinusoidal steady state representation, the system has been fixed in space for an infinite time. In a Gedankenexperiment, the material would be held in place and then released at some instant, with the associated force density distribution a predictor of motion. Physically and in an experiment, inertia or condensed-matter properties dictate when a material responds mechanically in a measurable way to incident radiation and hence deforms. The time scale for such motion will generally be large relative to the optical period, and hence the average sinusoidal steady state representation (or a time average over the carrier period with modulated light) becomes practical and simplifies the analysis. We consider time-harmonic, monochromatic fields with $\exp(-i\omega t)$ time convention for the inverse Fourier transform, where ω is the circular frequency. Consequently (5) becomes

$$\langle \mathbf{f} \rangle = \frac{\omega \mu_0}{2} \mathrm{Im}[\mathbf{P} \times \mathbf{H}^*] + \frac{1}{2} \mathrm{Re}[(\mathbf{P} \cdot \nabla)\mathbf{E}^*], \tag{6}$$

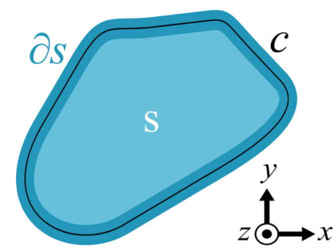

FIG. 1. Schematic showing a dielectric waveguide in free-space with an arbitrary cross-section in the x-y plane that is assumed uniform in the z-direction. The black contour c indicates the material boundary, the light-blue region shows the integration region s for calculating the bulk force, and the dark-blue region (assumed to be infinitesimally thin) shows the region of integration ∂s for calculating the surface force.

where $\langle \cdot \rangle$ is the time average operator, $\mathrm{Re}[\cdot]$ is the real part operator, and $\mathrm{Im}[\cdot]$ is the imaginary part operator, and all fields are now (complex) phasors. Here we have utilized the fact that for two time-harmonic functions, the time-average of their product is given as $\frac{1}{2}\mathrm{Re}[a(\mathbf{r})b^*(\mathbf{r})]$, assuming peak amplitudes for the sinusoids.

We apply (6) to calculate the time-averaged force density at each location within the structure. In this work, we restrict ourselves to waveguide structures that are uniform along the z-direction, as depicted in Fig. 1. To obtain the time-averaged force per unit length in z (referred to simply as force hereafter), we integrate the force density over the cross-section of the material, s, as

$$\langle \mathbf{F}^{\mathrm{bulk}} \rangle = \iint_s \langle \mathbf{f} \rangle ds. \tag{7}$$

The spatial derivative involved in the $\mathrm{Re}[(\mathbf{P} \cdot \nabla)\mathbf{E}^*]/2$ term in (6) results in a Dirac delta contribution in the force density for an interface and for the normal component of the electric field. This Dirac delta force density has been addressed physically and mathematically [12,37–39]. A force linked to this field step function is thus a surface force, and this becomes

$$\langle \mathbf{F}^{\mathrm{surf}} \rangle = \iint_{\partial s} \frac{1}{2} \mathrm{Re}[(\mathbf{P} \cdot \nabla)\mathbf{E}^*] ds, \tag{8}$$

where the region of integration is now over the infinitesimally thin strip of region along ∂s, the boundary of surface s. Note that the first term in (5) is finite across material boundaries, and therefore does not contribute when integrated over ∂s. The inclusion of the surface ("surf") force with the bulk force gives the "sum" force as

$$\langle \mathbf{F}^{\mathrm{sum}} \rangle = \langle \mathbf{F}^{\mathrm{bulk}} \rangle + \langle \mathbf{F}^{\mathrm{surf}} \rangle. \tag{9}$$

At each spatial point in the material, there is a torque density associated with the force density, relative to some reference point [14]. Assuming homogeneous material, we calculate the spatially dependent time-averaged torque density relative to a structure's center of mass as

$$\langle \boldsymbol{\tau} \rangle = \mathbf{r} \times \langle \mathbf{f} \rangle, \tag{10}$$

where $\mathbf{r}$ is the position vector originating at the center of mass. Following this, we obtain the torque on the structure by integrating over the material as

$$\langle \mathcal{T}^{\text{bulk}} \rangle = \int_s \langle \boldsymbol{\tau} \rangle ds. \tag{11}$$

If one considers the surface force, then there will also be a torque associated with the material boundary, which we calculate as

$$\langle \mathcal{T}^{\text{surf}} \rangle = \iint_{\partial s} \mathbf{r} \times \frac{1}{2}\text{Re}[(\mathbf{P} \cdot \nabla)\mathbf{E}^*] ds. \tag{12}$$

Similar to the sum force, the sum torque becomes

$$\langle \mathcal{T}^{\text{sum}} \rangle = \langle \mathcal{T}^{\text{bulk}} \rangle + \langle \mathcal{T}^{\text{surf}} \rangle. \tag{13}$$

In this work, we consider isotropic materials having a dielectric constant ϵ and refractive index (for nonmagnetic materials) of $n = \sqrt{\epsilon}$. Thus, $\mathbf{P} = \epsilon_0 \chi_E \mathbf{E}$ in the frequency domain, with the electric susceptibility $\chi_E = \epsilon - 1$. We present both the surface and bulk force contributions for completeness. Although including the surface force yields results consistent with those obtained by integration of the free space stress tensor around the waveguide—from volume integration and application of the divergence theorem to (2) (see Refs. [12,38,40])—the physical justification for the existence of such a surface force in real materials at optical frequencies remains an interesting question [37]. The Dirac delta force density is not needed to explain, for example, the water experiment done by Ashkin and Dziedzic [16] (see related discussions [35,41] and simulation results [14]). Additional experimental studies are needed to obtain information about near-surface force densities. The role of asymmetric waveguide force experiments is broached in Sec. V.

III. RELATIONSHIP BETWEEN EIGENMODE SYMMETRY AND OPTICAL FORCE DENSITY

We consider the optical waveguide depicted in Fig. 2(a) with symmetry in the y-direction but not in the x-direction, and a configuration with no planes of symmetry, as in Fig. 2(b). The confinement of the waveguide modes (indexed by n), with a propagation constant k_{zn} corresponding to the longitudinal variation $\exp(ik_{zn}z)$, arises from a dielectric core with dielectric constant ϵ embedded in a free-space background. In general, at some circular frequency ω, we have $\epsilon = \epsilon' + i\epsilon''$ and hence $k_z = k_z' + ik_z''$, with $\epsilon' > 1$ providing confinement and $\epsilon'' > 0$ representing loss [with $\exp(-i\omega t)$ time convention]. However, we will consider the lossless material case, and hence both ϵ and the eigenvalues for the waveguide modes, k_{zn}, are real. Assigning a coordinate reference to the plane of symmetry, geometrical symmetry is reflected in $\epsilon(x, y)$ with $x \to -x$ and $y \to -y$. By way of example, assigning $y = 0$ to the plane of symmetry in Fig. 2(a), shown as the red dotted line, we have $\epsilon(x, y) = \epsilon(x, -y)$. For a symmetric structure, the associated eigenmode fields must have an even or odd character around planes of symmetry, and this plays out in terms of the force density in (6) and hence the total force as the spatial integral of this density.

We should place symmetry or lack thereof, as it relates to the optical force density in dielectric waveguides, on a general theoretical footing. In particular, we inquire whether structural symmetry, which enforces mode symmetry, produces a symmetric force density that yields no net force along the direction of symmetry. We could then infer that a lack of symmetry leads to the possibility of a nonzero bulk force obtained using (7). Such a proof would show that symmetry precludes a net transverse force and hence a lack of symmetry does not. We present anecdotal numerical results that support this hypothesis.

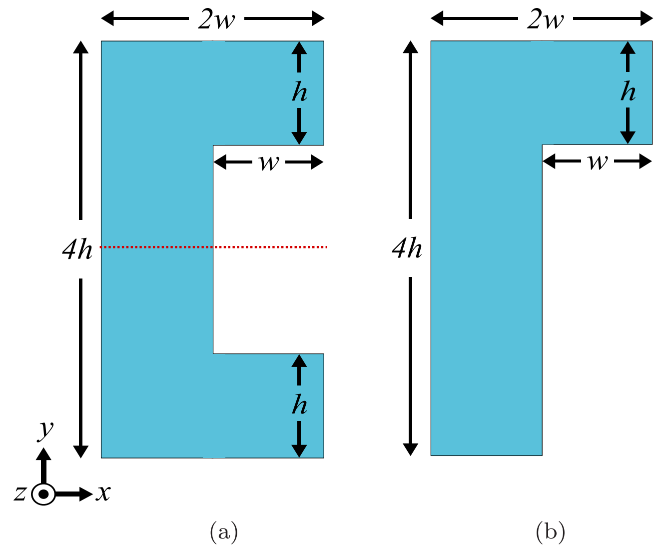

FIG. 2. Simulated silicon (Si) waveguide structures in free space with refractive index $n = 3.48$. (a) A double-ridge waveguide with symmetry in the y-direction but a lack of symmetry in the x-direction. The dotted red line indicates the plane of symmetry ($y = 0$). (b) A doubly asymmetric Si waveguide, with asymmetry along both axes. Both structures are assumed to be uniform and infinitely long in the propagation (z) direction.

Modes associated with dielectric waveguide structures having finite dimensions in the two orthogonal transverse coordinates such as those in Fig. 2 require all six electromagnetic field components to satisfy the boundary conditions. Maxwell's curl equations in this situation can be written as

$$\nabla \times \mathbf{H}_n = -i\omega\epsilon_0\epsilon\mathbf{E}_n, \tag{14}$$

$$\nabla \times \mathbf{E}_n = i\omega\mu_0\mathbf{H}_n, \tag{15}$$

with (14) being Ampere's law and (15) Faraday's law, and $\mathbf{E}_n$ and $\mathbf{H}_n$ the nth eigenmode electric and magnetic fields, respectively. Here, we assume the frequency domain form is generated based on $\exp(-i\omega t)$ in the inverse Fourier transform and hence $\partial/\partial t \to -i\omega$. With $\exp(ik_{zn}z)$ phase propagation along z, the eigenmode fields can be expressed as

$$\mathbf{E}_n = [\hat{\mathbf{x}}e_{xn}(x, y) + \hat{\mathbf{y}}e_{yn}(x, y) + \hat{\mathbf{z}}e_{zn}(x, y)]e^{ik_{zn}z}, \tag{16}$$

$$\mathbf{H}_n = [\hat{\mathbf{x}}h_{xn}(x, y) + \hat{\mathbf{y}}h_{yn}(x, y) + \hat{\mathbf{z}}h_{zn}(x, y)]e^{ik_{zn}z}. \tag{17}$$

Incorporating (16) and (17) into (14) and (15), the transverse field components can be expressed in terms of the longitudinal components as

$$h_{xn} = \frac{i}{k_{cn}^2}\left(-\omega\epsilon_0\epsilon\frac{\partial e_{zn}}{\partial y} + k_{zn}\frac{\partial h_{zn}}{\partial x}\right), \tag{18}$$

$$h_{yn} = \frac{i}{k_{cn}^2}\left(\omega\epsilon_0\epsilon\frac{\partial e_{zn}}{\partial x} + k_{zn}\frac{\partial h_{zn}}{\partial y}\right), \tag{19}$$

$$e_{xn} = \frac{i}{k_{cn}^2}\left(k_{zn}\frac{\partial e_{zn}}{\partial x} + \omega\mu_0\frac{\partial h_{zn}}{\partial y}\right), \tag{20}$$

$$e_{yn} = \frac{i}{k_{cn}^2}\left(k_{zn}\frac{\partial e_{zn}}{\partial y} - \omega\mu_0\frac{\partial h_{zn}}{\partial x}\right), \tag{21}$$

where $k_{cn}^2 = k^2 - k_{zn}^2$, with $k^2 = \omega^2\epsilon/c^2$. Thus, $e_{zn}(x, y)$ and $h_{zn}(x, y)$ contain the necessary information to understand field and force density symmetries associated with each eigenmode. Should symmetry exist with respect to direction x/y (read as x or y), then all field components must be odd or even about x/y. This, along with (18)–(21), imposes the condition that $e_{zn}(x/y)$ and $h_{zn}(x/y)$ have opposite symmetry, i.e., modes with $e_{zn}(x/y)$ even have $h_{zn}(x/y)$ odd, and those with $e_{zn}(x/y)$ odd have $h_{zn}(x/y)$ even. This leads to four symmetry classes:

(1) Class (i): $e_{zn}(y)$ odd and $h_{zn}(y)$ even.
(2) Class (ii): $e_{zn}(y)$ even and $h_{zn}(y)$ odd.
(3) Class (iii): $e_{zn}(x)$ odd and $h_{zn}(x)$ even.
(4) Class (iv): $e_{zn}(x)$ even and $h_{zn}(x)$ odd.

Based on our example case in Fig. 2(a), we focus on Class (i) and Class (ii), that is, symmetry with respect to $y = 0$. This yields

(1) Class (i): Odd $e_{zn}(y), e_{xn}(y)$ and $h_{yn}(y)$; even $h_{zn}(y)$, $h_{xn}(y)$ and $e_{yn}(y)$.
(2) Class (ii): Even $e_{zn}(y), e_{xn}(y)$ and $h_{yn}(y)$; odd $h_{zn}(y)$, $h_{xn}(y)$ and $e_{yn}(y)$.

Given these symmetry properties of the fields, each term in (6) can be analyzed to determine the symmetry of the time-averaged force density associated with each mode. Mode spatial orthogonality, fundamentally a field concept, can be extended to the force density (as can be done with the power). Therefore, we consider the two terms in (6) associated with the nth eigenmode and expand the vector components as

$$[\mathbf{P}\times\mathbf{H}^*]_n = \epsilon_0\chi_E\begin{bmatrix} e_{yn}h_{zn}^* - e_{zn}h_{yn}^* \\ e_{zn}h_{xn}^* - e_{xn}h_{zn}^* \\ e_{xn}h_{yn}^* - e_{yn}h_{xn}^*\end{bmatrix}, \tag{22}$$

and

$$[(\mathbf{P}\cdot\nabla)\mathbf{E}^*]_n = \epsilon_0\chi_E\begin{bmatrix} e_{xn}\frac{\partial e_{xn}^*}{\partial x} + e_{yn}\frac{\partial e_{xn}^*}{\partial y} - ik_{zn}e_{zn}e_{xn}^* \\ e_{xn}\frac{\partial e_{yn}^*}{\partial x} + e_{yn}\frac{\partial e_{yn}^*}{\partial y} - ik_{zn}e_{zn}e_{yn}^* \\ e_{xn}\frac{\partial e_{zn}^*}{\partial x} + e_{yn}\frac{\partial e_{zn}^*}{\partial y} - ik_{zn}e_{zn}e_{zn}^*\end{bmatrix}. \tag{23}$$

In (23), we have used $\partial\mathbf{E}_n^*/\partial z = -ik_{zn}\mathbf{E}_n^*$. Incorporating (22) and (23) into (6), we obtain the time-averaged transverse force density components associated with each eigenmode as

$$\begin{aligned}\langle f_{xn}(x, y)\rangle = {} & \frac{\omega\mu_0}{2}\mathrm{Im}\{\epsilon_0\chi_E(e_{yn}h_{zn}^* - e_{zn}h_{yn}^*)\} \\ & + \frac{1}{2}\mathrm{Re}\left\{\epsilon_0\chi_E\left[e_{xn}\frac{\partial e_{xn}^*}{\partial x} + e_{yn}\frac{\partial e_{xn}^*}{\partial y} - ik_{zn}e_{zn}e_{xn}^*\right]\right\},\end{aligned} \tag{24}$$

and

$$\begin{aligned}\langle f_{yn}(x, y)\rangle = {} & \frac{\omega\mu_0}{2}\mathrm{Im}\{\epsilon_0\chi_E(e_{zn}h_{xn}^* - e_{xn}h_{zn}^*)\} \\ & + \frac{1}{2}\mathrm{Re}\left\{\epsilon_0\chi_E\left[e_{xn}\frac{\partial e_{yn}^*}{\partial x} + e_{yn}\frac{\partial e_{yn}^*}{\partial y} - ik_{zn}e_{zn}e_{yn}^*\right]\right\}.\end{aligned} \tag{25}$$

Note that $\langle f_{xn}(x, y)\rangle$ and $\langle f_{yn}(x, y)\rangle$ are independent of axial position for the lossless waveguide case. However, regardless of the presence of dissipative loss in the eigenmodes, the transverse description of the force density symmetry remains valid. Interestingly, the force density spatial distribution depends on the eigenvalue, k_{zn}.

Referring to the field symmetries for Classes (i) and (ii) and Fig. 2(a), we find that for both classes

$$\langle f_{xn}(x, y)\rangle = \langle f_{xn}(x, -y)\rangle \rightarrow \text{Even}, \tag{26}$$

$$\langle f_{yn}(x, y)\rangle = -\langle f_{yn}(x, -y)\rangle \rightarrow \text{Odd}. \tag{27}$$

The bulk force from each eigenmode $\langle\mathbf{F}_n^{\text{bulk}}\rangle$ on the structure is obtained by integrating (24) and (25) over the cross section of the waveguide in accordance with (7). As a result, the electromagnetic force in the direction of symmetry vanishes upon integration over the transverse plane. A similar argument applies to structures symmetric about $x = 0$, where $\langle f_{xn}\rangle$ becomes odd about $x = 0$ and the net force in the x-direction vanishes. Thus, waveguide structures with symmetry in both transverse directions, such as rectangular or elliptical waveguides, do not experience a net force due to propagating modes, as $\langle f_{xn}(x, y)\rangle = -\langle f_{xn}(-x, y)\rangle$ and $\langle f_{yn}(x, y)\rangle = -\langle f_{yn}(x, -y)\rangle$. For structures that are symmetric in y, but lack symmetry in the x-direction, such as the geometry shown in Fig. 2(a), $\langle f_{xn}(x, y)\rangle$ is even in y and does not possess any particular symmetry in x. Thus, such structures cannot exhibit a net force in the y-direction, but in general may experience a nonzero force in the x-direction. For waveguides with broken symmetry in both transverse directions [Fig. 2(b)], both transverse force density components are asymmetric, and therefore the net force magnitude and direction are dictated by the asymmetry of the fields resulting from the structural asymmetry.

IV. SIMULATED FORCE AND TORQUE FOR ASYMMETRIC WAVEGUIDES

A. Eigenmode numerical simulations

We numerically study the force density associated with the eigenmodes of the dielectric waveguide structures in Fig. 2. In the examples considered, a free-space wavelength of $\lambda = 1550$ nm is used and silicon (Si) with a lossless (hence real) refractive index of $n = 3.48$ is assumed, and the background medium is free space. The eigenmodes are computed using two-dimensional (2D) finite element method (FEM) simulations [42]. The transverse domain is terminated using a scattering boundary condition to model an infinite free-space domain. The time-averaged Poynting vector along the propagation direction for each mode, $\langle S_{zn}\rangle = \frac{1}{2}\mathrm{Re}(\mathbf{E}_n \times \mathbf{H}_n^*)\cdot\hat{\mathbf{z}}$, is integrated over the transverse simulation domain to calculate the guided power. Using this

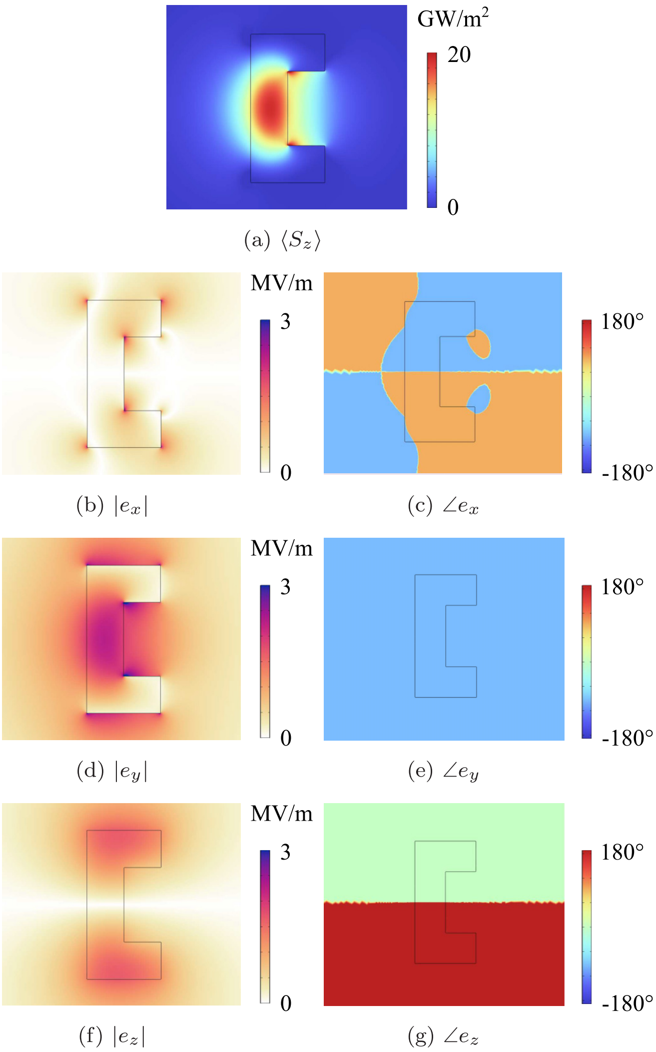

FIG. 3. Simulated Poynting vector and fields for the only guided mode in the double-ridge Si waveguide of Fig. 2(a), with $h = w = 100$ nm, mode power of 1 mW, and at a free-space wavelength of 1550 nm, yielding a mode index (k_z/k_0, with k_0 the free-space wave number) of $n_{\mathrm{eff}} = 1.44$: (a) The z component of the time-averaged Poynting vector, $\langle S_z\rangle$; (b) $|e_x|$; (c) $\angle e_x$; (d) $|e_y|$; (e) $\angle e_y$; (f) $|e_z|$; (g) $\angle e_z$, indicating Class (i).

power, the eigenmodes are normalized such that the total guided power is 1 mW for each mode. Further details about the simulation methodology and force density calculation are available in Appendix A.

B. Force and torque with broken symmetry in one dimension

We first consider the double-ridge waveguide in Fig. 2(a) and the situation of symmetry in the y-direction and asymmetry with respect to x, with dimensions $h = w = 100$ nm. Figure 3(a) presents $\langle S_z\rangle$ for the only guided mode ($n = 1$) with an effective mode index (ratio of the propagation constant of the mode and the free-space wave number) $k_z/k_0 = n_{\mathrm{eff}} = 1.44$, with $k_0 = \omega/c$. As there is only one eigenmode for this structure, we suppress the mode index identifier for this case. The confinement of the mode within the waveguide region is apparent from the power density in Fig. 3(a).

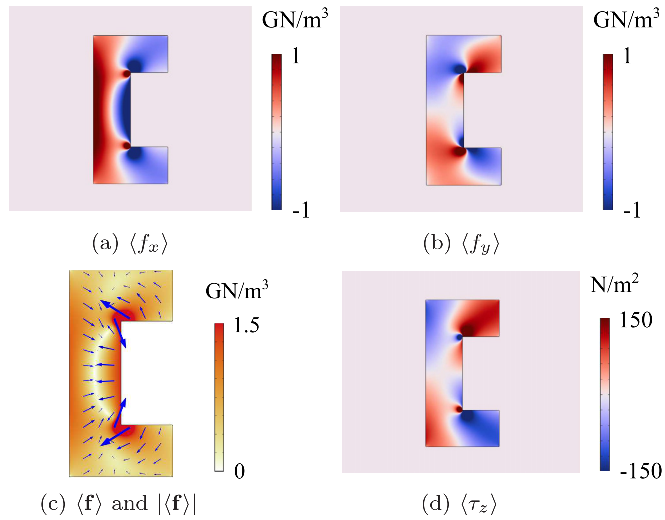

FIG. 4. Simulated force and torque density for the single guided mode in the double-ridge Si waveguide of Fig. 2(a), with $h = w = 100$ nm, mode power of 1 mW, and at a free-space wavelength of 1550 nm: (a) $\langle f_x\rangle$; (b) $\langle f_y\rangle$; (c) $\langle \mathbf{f}\rangle$ and $|\langle \mathbf{f}\rangle|$; and (d) $\langle \tau_z\rangle$. The index n has been suppressed because there is only one mode. Note that the symmetries in the force density components are commensurate with the description provided in Sec. III and Case (i): No net force in the direction of symmetry (the y-direction). The vector plot of the force density shows that the central region experiences compression and the torque indicates that the ridges experience a bending force.

The electric field magnitudes and phases are presented in Figs. 3(b)–3(g). Note that the field solution falls into symmetry Class (i), as discussed in Sec. III; $e_z(y)$ is odd.

Figures 4(a) and 4(b) show the x- and y-components of the time-averaged force density, respectively, calculated using (6). As discussed in Sec. III, $\langle f_x(y)\rangle$ is even in y, the direction having geometric symmetry, and has no particular symmetry in x, yielding a net force $\langle F_x^{\mathrm{bulk}}\rangle = -0.61\ \mu\mathrm{N/m}$, whereas the antisymmetric $\langle f_y\rangle$ leads to cancellation and a net zero force in the y-direction. The numerical integration of $\langle f_y\rangle$ provides a value that is several orders of magnitude smaller than $\langle F_x^{\mathrm{bulk}}\rangle$ (see Appendix A), and $\langle f_y(y)\rangle$ in Fig. 4(b) is clearly antisymmetric. We therefore conclude that the small nonzero value of $\langle F_y^{\mathrm{bulk}}\rangle$ is due to numerical precision, inherent in any computational solution, and therefore interpret it as zero, i.e., $\langle F_y^{\mathrm{bulk}}\rangle = 0\ \mu\mathrm{N/m}$. Figure 4(c) shows the time-averaged optical force density vector, with the blue arrows indicating the magnitude and direction of the force density vector $\langle \mathbf{f}\rangle$ at the tail of each arrow. The background color plot indicates the magnitude of force density, $|\langle \mathbf{f}\rangle|$. Note the white region near the center of the waveguide, where a compressive force is experienced.

As $\langle f_x(y)\rangle$ and $\langle f_y(y)\rangle$ exhibit even and odd symmetry, respectively, about $y = 0$, the torque density, $\langle \tau_z\rangle$, calculated using (10), must be odd about y. This is seen in Fig. 4(d), where the time-averaged z-directed torque density is determined as

$$\langle \tau_z\rangle = (x'\langle f_y\rangle - y'\langle f_x\rangle), \tag{28}$$

where x' and y' are coordinates measured from the center of mass. This yields a $\langle \tau_z\rangle$ that is predominantly positive in the

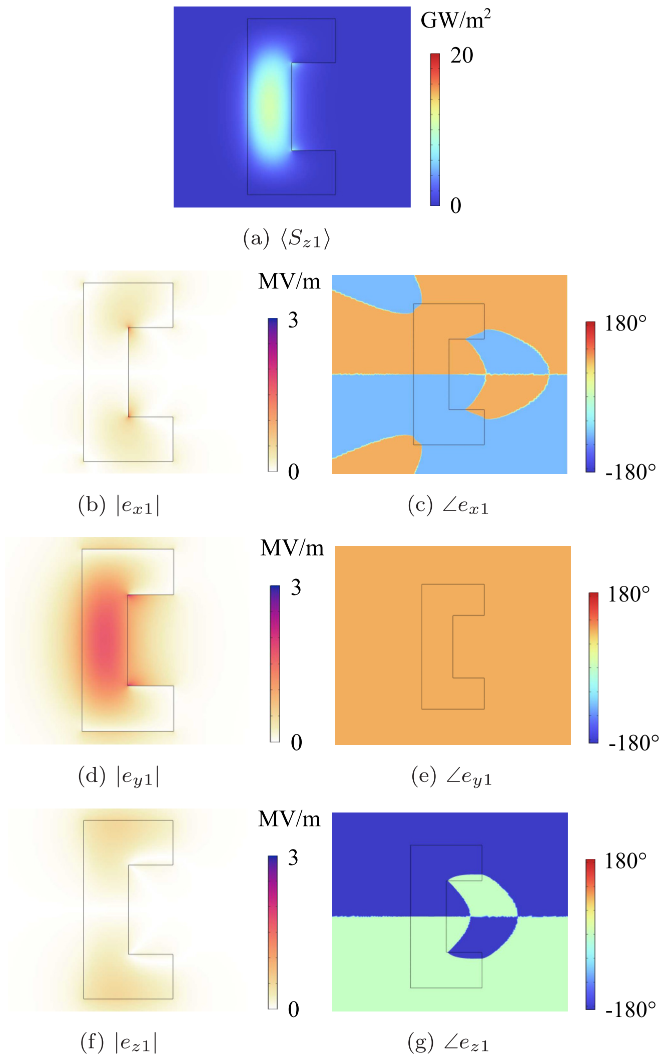

FIG. 5. Simulated power density and fields for the fundamental mode ($n_{\text{eff}} = 2.62$) in the enlarged double-ridge Si waveguide structure of Fig. 2(a) having $h = w = 200$ nm, again a free-space wavelength of 1550 nm: (a) $\langle S_{z1}\rangle$; (b) $|e_{x1}|$; (c) $\angle e_{x1}$; (d) $|e_{y1}|$; (e) $\angle e_{y1}$; (f) $|e_{z1}|$; and (g) $\angle e_{z1}$. The electric field indicates Class (i). The fields for each mode are scaled so that the guided power is 1 mW.

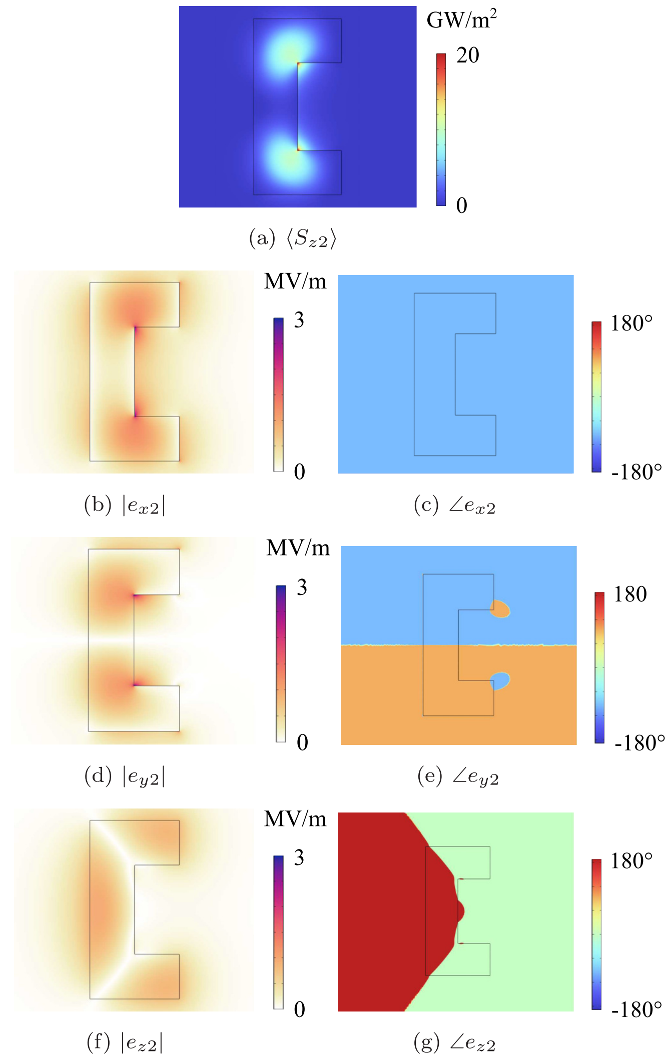

FIG. 6. Simulated power density and fields for the second mode ($n_{\text{eff}} = 2.30$) in the enlarged double-ridge Si waveguide structure of Fig. 2(a) having $h = w = 200$ nm and again a free-space wavelength of 1550 nm: (a) $\langle S_{z2}\rangle$; (b) $|e_{x2}|$; (c) $\angle e_{x2}$; (d) $|e_{y2}|$; (e) $\angle e_{y2}$; (f) $|e_{z2}|$; and (g) $\angle e_{z2}$. The electric field indicates Class (ii). The fields for each mode are scaled so that the guided power is 1 mW.

upper region (hence counterclockwise) and negative in the lower half (clockwise). For this waveguide, there is no net torque and hence no net rotational force. However, as is clear in Fig. 4(d), there are local regions within the structure that will experience a torque and that the two protruding ridge regions of the waveguide will experience a bending force away from each other.

To explore the role of mode order on force behavior, we consider the double-ridge structure enlarged by a factor of 2 in all dimensions, that is, $h = w = 200$ nm, referring to Fig. 2(a). This proportional enlargement preserves the overall aspect ratio and symmetry features while enabling the emergence of higher-order guided modes. Under these conditions, the waveguide supports a total of four guided modes, and for our analysis we consider the first two modes, the fundamental mode [$n = 1$ with symmetry Class (i) and $n_{\text{eff}} = 2.62$] and the second mode [$n = 2$ with symmetry Class (ii) and $n_{\text{eff}} = 2.30$]. Figures 5(a) and 6(a) show $\langle S_{zn}\rangle$ for the first and second eigenmodes, respectively. For the fundamental mode, most of the power is confined near the center region, and for the second mode, the power flow is concentrated near the two ridges. The magnitudes and phases of the electric field components of the fundamental mode are shown in Figs. 5(b)–5(g) and for the second mode in Figs. 6(b)–6(g). Note that the two modes have opposite parity for each field component with respect to y. As one would expect, the fundamental mode (Fig. 5, left column) has the same mode shape as that from the previous structure (Fig. 3), since we have changed only size and not shape of the waveguide. The only difference is smaller amplitudes for the enlarged structure, as the same power is confined over a larger region.

Figures 7(a) and 7(b) show the force density vectors $\langle \mathbf{f}_n\rangle$ and magnitudes $|\langle \mathbf{f}_n\rangle|$ (as a color map) associated with the two lowest-order modes for the larger double-ridge Si waveg-

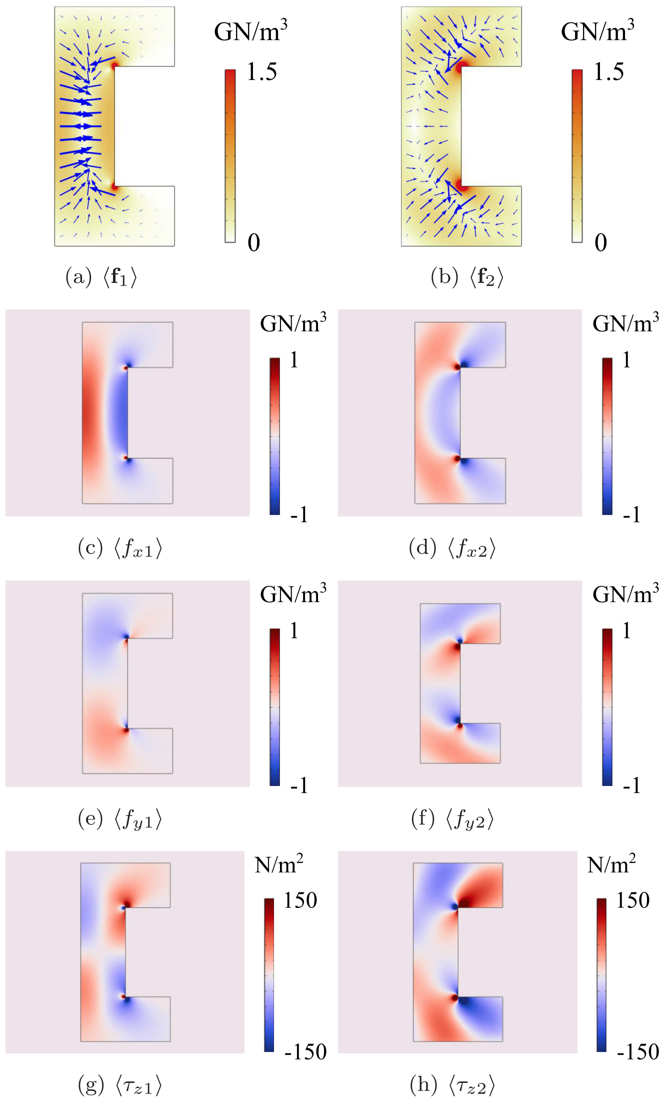

FIG. 7. Simulated force densities and torques for the double-ridge Si waveguide of Fig. 2(a) with $h = w = 200$ nm, with the lowest order mode 1 on the left and the next higher-order mode 2 on the right and with a free-space wavelength of 1550 nm: (a), (b) $\langle \mathbf{f}_n \rangle$ and $|\langle \mathbf{f}_n \rangle|$; (c), (d) $\langle f_{xn} \rangle$; (e), (f) $\langle f_{yn} \rangle$; and (g), (h) $\langle \tau_{zn} \rangle$. For both modes, $\langle f_{xn} \rangle$ are even and $\langle f_{yn} \rangle$ are odd functions of y. Therefore, $\langle \tau_{zn} \rangle$ are also odd functions of y for both modes. Each mode has a power of 1 mW.

uide. These force density plots reveal a clear asymmetry in the x-direction for both modes. This x-directed force density asymmetry is further illustrated in Figs. 7(c) and 7(d), which show $\langle f_{xn} \rangle$. The lateral asymmetry leads to a nonzero net force of $\langle F_{x1}^{\text{bulk}} \rangle = -0.20$ μN/m for the fundamental mode and $\langle F_{x2}^{\text{bulk}} \rangle = -1.18$ μN/m in the case of the second mode. Note that the higher-order mode has significantly larger transverse force compared to the fundamental mode. In our simulations, we noticed a general trend, for the situations considered, that higher-order modes exert larger net forces for a given geometry and each mode scaled to have the same power. In contrast, $\langle f_{yn}(y) \rangle$ shown in Figs. 7(e) and 7(f) remains antisymmetric, resulting in $\langle F_{yn}^{\text{bulk}} \rangle = 0$ μN/m. Structure and hence mode symmetry forces a zero net force in the direction with symmetry, regardless of the mode order. The corresponding torque densities $\langle \tau_{zn} \rangle$, presented in Figs. 7(g) and 7(h), have odd symmetry about y as expected, and thus result in $\langle \mathcal{T}_{zn}^{\text{bulk}} \rangle = 0\,\text{N}$.

A notable outcome of the theory described in Sec. III, in particular (24) and (25), is the dependence of the force density on the eigenvalue k_{zn}, and therefore the effective mode index ($k_z = n_{\text{eff}} k_0$). This effect presents itself as subtle differences between the force and torque densities in Fig. 4 and that of the fundamental mode in Fig. 7 (left column), as they have different n_{eff}. While the differences are small in our case, the results do establish the general concept that waveguides with different sizes and the same geometric and eigenmode shape will experience a different force density distribution. This understanding should prove useful as a design concept for studying and utilizing optomechanical effects.

All of the simulated eigenmode fields have electric field components that are perpendicular to the interfaces and hence a nonzero $\langle \mathbf{F}_n^{\text{surf}} \rangle$, referring to (8), because of the mathematical Dirac delta in the force density. When the surface force density term is integrated across and along the waveguide boundary and added to $\langle \mathbf{F}_n^{\text{bulk}} \rangle$ to form $\langle \mathbf{F}_n^{\text{sum}} \rangle$, the total transverse force components become zero, regardless of the presence or lack of symmetry. Thus, $\langle \mathbf{F}_n^{\text{sum}} \rangle = 0$ for this waveguide system.

C. Force and torque with broken symmetry in two dimensions

We next consider the single-ridge Si waveguide structure of Fig. 2(b), which, unlike the double-ridge waveguide, lacks symmetry in both transverse directions. Symmetry in the y-direction is broken by removing the lower ridge from the double-ridge waveguide (preserving the total height). We choose $h = w = 100$ nm and again a free-space wavelength of 1550 nm. Figure 8(a) presents $\langle S_z \rangle$ for the only propagating mode ($n_{\text{eff}} = 1.30$). The associated electric field components are shown in Figs. 8(b)–8(g), and it is apparent that there is no plane of symmetry. Hence, both $\langle f_x \rangle$ and $\langle f_y \rangle$ in Figs. 9(a) and 9(b) lack symmetry and therefore lead to net forces of $\langle F_x^{\text{bulk}} \rangle = -0.28$ μN/m and $\langle F_y^{\text{bulk}} \rangle = 0.92$ μN/m. The vector force density is shown in Fig. 9(c), shedding light on the torque density in Fig. 9(d). Note that asymmetry in $\langle f_x \rangle$ and $\langle f_y \rangle$ leads to asymmetry in the $\langle \tau_z \rangle$ results of Fig. 9(d). This yields a net torque on this waveguide of $\langle \mathcal{T}_z \rangle = 49.42$ fN. With incorporation of the surface Dirac component of the force density, both transverse components of $\langle \mathbf{F}^{\text{sum}} \rangle$ are zero, because the surface force terms exactly cancel the bulk force, and the total torque, $\langle \mathcal{T}^{\text{sum}} \rangle$, is zero (so the surface and bulk torques are equal in magnitude and in opposite directions).

D. Summary of force and torque for waveguides with broken symmetry

To consolidate the findings across all waveguide configurations, we provide a comparative summary of the bulk optical force and torque results in Table I. The inclusion of the surface force takes the total transverse force to zero, canceling the bulk force, and results in no net torque. Even though including the surface contribution predicts no net force or torque, the internal force and torque distribution would still be expected to lead to deformation of the structure.

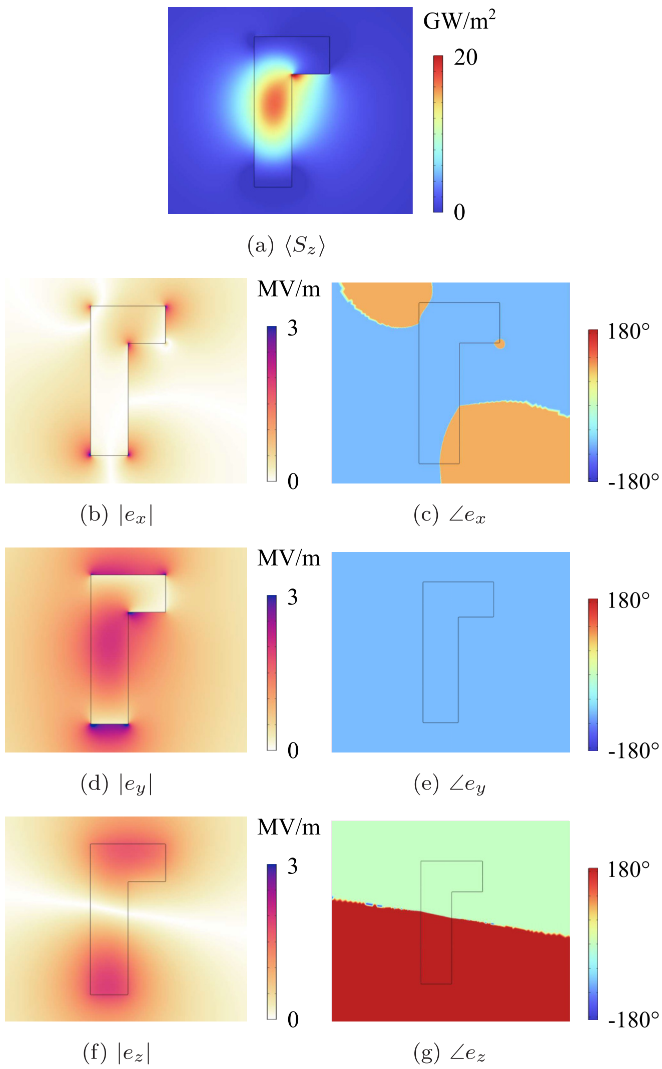

FIG. 8. Simulated results for the propagating mode for the single-ridge Si waveguide of Fig. 2(b) with $h = w = 100$ nm and a free-space wavelength of 1550 nm ($n_{\mathrm{eff}} = 1.30$): (a) $\langle S_z \rangle$; (b) $|e_x|$; (c) $\angle e_x$; (d) $|e_y|$; (e) $\angle e_y$; (f) $|e_z|$; (g) $\angle e_z$. We have suppressed the index n because there is only one eigenmode. Note that the electric field components lack any particular symmetry, leading to asymmetry in the force density components.

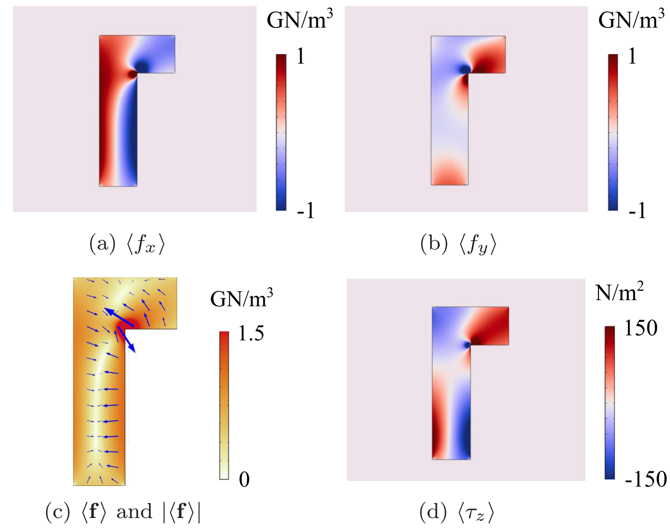

FIG. 9. Simulated force and torque density for the single-ridge Si waveguide of Fig. 2(b) with $h = w = 100$ nm and a free-space wavelength of 1550 nm: (a) $\langle f_x \rangle$; (b) $\langle f_y \rangle$; (c) $\langle \mathbf{f} \rangle$ and $|\langle \mathbf{f} \rangle|$; and (d) $\langle \tau_z \rangle$. The asymmetry in both force density components leads to a net torque.

In the double-ridge structure of Fig. 2(a), the notch induces an imbalance in the lateral force density, $\langle f_{xn} \rangle$, while maintaining antisymmetry in $\langle f_{yn} \rangle$ and $\langle \tau_{zn} \rangle$ [Fig. 4(d)]. The net force ($\langle F_{xn}^{\mathrm{bulk}} \rangle$) arises from structural asymmetry in that dimension. For the enlarged double-ridge waveguide, the two guided modes provide a comparison that emphasizes the interplay between spatial confinement, mode order, and mechanical response (Fig. 7). The trend observed is that (for fixed geometry and power) higher order modes provide a stronger force, which illustrates that mode selection or control can be used to tune the magnitude and spatial distribution of the force.

The single-ridge structure of Fig. 2(b) demonstrates that simultaneous asymmetry in both transverse directions yields not only significant transverse forces, but also appreciable torque (Fig. 9). This behavior suggests that asymmetry in two transverse dimensions can be exploited to rotate waveguide components.

E. Plausibility of transverse force measurement

To estimate the physical deformation of a waveguide due to the forces found in this work, we use Euler-Bernoulli beam theory [43]. The maximum deflection of a beam of length l with fixed ends, when it experiences a uniform force per unit length p, is

$$u_{\max} = \frac{pl^4}{384\mathcal{E}I}, \tag{29}$$

where $\mathcal{E}$ is the elastic modulus of the material and I is the second moment of inertia of the structure's cross section. The derivation for (29) is provided in Appendix B. Assuming $l = 500$ μm, $\mathcal{E} = 170$ GPa (for Si), a square cross section with 400 nm sides, and $p = 0.61$ μN/m (from Table I), we find $u_{\max} = 273.7$ nm (with a power of 1 mW) from the bulk force. This indicates that suspended waveguides may be engineered

TABLE I. Comparison of the "bulk" optical forces and torques for different waveguide configurations. The superscript "bulk" is omitted for compactness. The double-ridge and enlarged cases are for the geometry in Fig. 2(a) and the single-ridge is the situation in Fig. 2(b). The double-ridge results are shown in Fig. 4, the enlarged (double-ridge) waveguide data for the two lowest order modes is taken from Fig. 7, and the single-ridge waveguide is considered in Fig. 9.

Structure/Mode	$\langle F_x \rangle$ [μN/m]	$\langle F_y \rangle$ [μN/m]	$\langle \mathcal{T}_z \rangle$ [fN]
Double-ridge	−0.61	0	0
Enlarged ($n = 1$)	−0.20	0	0
Enlarged ($n = 2$)	−1.18	0	0
Single-ridge	−0.28	0.92	49.42

to allow significant and measurable deformation due to the optical force from the propagating modes.

V. DISCUSSION

Investigation of the force and torque density throughout a waveguide provides the fundamental way to model expected deformation. The results presented highlight the critical role of geometric asymmetry and mode selection in shaping the optical force landscape in dielectric waveguides. Introducing asymmetry along a particular dimension results in an asymmetric distribution in the component of the force density in that direction, and therefore yields a force. On the contrary, structure symmetry, regardless of the field parity, leads to an antisymmetric force density along that direction and hence no net bulk force. We also learn that higher-order eigenmodes tend to exert a large bulk force given a fixed propagating mode power. A particular waveguide may have multiple modes excited. This means that regulation of the total force can be achieved through relative excitation of the set of propagating modes. Furthermore, the dependence of the force density associated with each mode on the respective eigenvalue is revealed, which could be leveraged to design structures for optomechanical experiments and applications. With asymmetry in both transverse directions, it may be possible to rotate the structure using optical force from the guided modes. With these effects in mind, integrated optomechanical structures could be engineered. From a device perspective, these results suggest a pathway for designing waveguides and photonic structures that achieve optical actuation through optical force. The forces demonstrated here should provide significant deformation to waveguide structures, and therefore could be leveraged for device concepts.

We now address the physical implications of our results and motivate experiments along these lines. The model for the force density used in (6) applies with the structure in a fixed position while the fields are established. Practically, this role may be fulfilled by inertia. However, the situation in an experiment may require a more sophisticated analysis. Our work suggests that the deformation due to asymmetry is measurable, and hence an experiment along this line should be interesting. In all waveguide cases studied, the surface (Dirac delta density) term cancels the bulk force entirely, leading to zero sum force and torque. If the model in (5) holds and if there is transverse waveguide motion, then this will imply that the Dirac term does not apply, or that the weight of such a term must be revised from the classical boundary condition. Interestingly, the bulk term implies motion in a particular direction and the surface term in exactly the opposite direction. With modern fabrication capabilities, it is possible to fabricate suitable suspended waveguide structures [17,44], and laser Doppler vibrometry (LDV) [45] or optical beam deflection [46] could be used to detect nanometer-scale deformation in the waveguide due to modulated light. Such an experiment would provide insight into the force density near material interfaces based on the presence or absence of deflection and its direction. Even if the net transverse force on asymmetric solid state waveguides was found to be zero, the asymmetries in the bulk force density in soft materials should result in commensurate motion, and asymmetric phonon modes in optical waveguides with rigid materials should also prove interesting.

Mathematical and physical aspects of the Dirac delta force density in relation to conservation requirements at boundaries have been treated previously [37]. With light incident from free space onto a material, the Dirac delta contribution is always directed outwards and in the direction opposite the incident light and the corresponding free-space photon momentum. This implies that as a photon enters the material from free space, it would exert a pulling force on the atoms near the interface (see the treatment related to ultrafast laser light in structured material [39]). Nonclassical and nonlocal (in space) models may be needed to fully describe the force density over small length scales and hence near material interfaces. For example, discrete interaction models [47,48], where the response of each atom is considered separately, have been used to study the optical response of ultrafine metallic structures. Such a model could be incorporated with optical force density theory to calculate the force on each atom and hence provide insight into photon-atom momentum exchange near material interfaces.

The application prospects suggested by this work include those related to integrated optical components based on concepts that exploit asymmetry in optomechanics. For example, asymmetry in a single waveguide might be used for tuning, either by propagating-mode-induced stress or by adjusting waveguide proximity to a neighboring element [31] to modulate coupling. This effect may be used in an optical coupler or switch, where one of two waveguides is suspended and can be moved by optical force. By breaking symmetry along both transverse axes, we observe not only forces in both direction, but also a nonzero net torque, introducing the possibility of rotational manipulation of waveguides using guided light. Such torque could be regulated through mode control (and potentially geometry control) for actuation or switching. With reference to Fig. 4(c), in principle, strain could be exploited to engineer spatially varying material properties. Although continuous-wave illumination may not generate sufficient strain to induce these effects, the higher field amplitudes from pulsed excitation could enable nonlinear responses of practical interest. Finally, as indicated in Fig. 4(d), the guided mode can reshape the local geometry in a mode-specific manner, opening opportunities for the targeted excitation of vibrational modes. Thus, structure asymmetry could be utilized with impulsive stimulated Raman scattering to excite particular phonon-polariton waves in ferroelectrics [49].

Power leakage for the force and torque results shown is negligible (see Appendix A) and should ideally be zero. We have thus described a net transverse force due to guided waveguide modes and associated with waveguide asymmetry. However, waveguide excitation could involve some finite number of propagating modes and leakage. An excitation having 2D symmetry in a waveguide with 2D symmetry would have leakage also preserving these symmetries. As a result, leakage would result in no net force, i.e., there would be no net recoil in the waveguide as photons are lost. However, with for example a point source excitation in an asymmetric waveguide, we would expect a net recoil force from leakage in the direction of asymmetry. This would be a situation where a force results from radiative loss due to asymmetry.

Experimentally, this could be achieved with a small fiber tip exciting an optical waveguide with some propagating mode spectrum. Such leakage could function in reverse, due to reciprocity, and this may provide for sensing applications.

VI. CONCLUSION

We have demonstrated that it may be possible to exert a transverse force on a lossless dielectric waveguide from propagating waveguide modes by building asymmetry into the structure. A waveguide could thus experience a net force in the direction of the asymmetry due to the asymmetric mode shapes. We also predict that waveguides with asymmetry in multiple transverse directions may experience a net torque, resulting in rotation. This work presents opportunities for applications in integrated photonics as well as experiments that may resolve important issues regarding the force density near material interfaces.

ACKNOWLEDGMENTS

This work was supported by the Defense Advanced Research Projects Agency (Grant No. W911NF-23-1-0043), the Army Research Office (Grant No. W911NF-22-2-0245), the Air Force Office of Scientific Research (Grant No. FA9550-23-1-0542), and the National Science Foundation (Grant No. 1927822). The procedure for the numerical implementation of the Dirac delta force density was developed by Dr. Adam Behnke during his Ph.D. work at Purdue.

DATA AVAILABILITY

The data that support the findings of this article are openly available [50]; embargo periods may apply.

APPENDIX A: WAVEGUIDE SIMULATION METHODOLOGY

We provide some additional details relating to the numerical simulations used to generate the results presented. The eigenmode simulations in Sec. IV were performed using the mode analysis tool in COMSOL Multiphysics [42]. Mesh element sizes were made sufficiently small, based on convergence studies using the bulk force on the structure as the metric. All corners were rounded to remove field singularities. Power leakage for the results shown are negligible, as established by calculating the power flow through a closed contour around the waveguide—as should be the case for these waveguide eigenmodes. However, because the eigenvalues and corresponding eigenfunctions are obtained numerically, they are subject to computational precision. We find that the power leakage is more than 125 dB below 1 mW, the normalized power used for each guided mode considered. The influence of this computational error on the net transverse force can be appraised by the integral of the stress tensor in free space and around the waveguide. Relative to the net transverse force we find due to asymmetry, the stress tensor (that encompasses the Dirac force density at the surface through the divergence theorem) indicates a time-averaged force more than 58 dB below the bulk forces found.

APPENDIX B: BEAM DEFLECTION UNDER UNIFORM LOAD

We provide the derivation for (29), which is used to estimate the expected deflection of the waveguide structures due to the force from a propagating mode. This deflection estimate is based on Euler-Bernoulli beam theory [43]. For a beam experiencing transverse loads, the governing equation for transverse deflection under this theory is

$$\frac{d^2}{dz^2}\mathcal{E}I\frac{d^2}{dz^2}u(z) = p(z), \tag{B1}$$

where z is the axis along the beam, $u(z)$ is the deflection of the beam, $p(z)$ is the force per unit length on the structure, $\mathcal{E}$ is the elastic modulus of the material, and I is the second moment of inertia of the beam's cross section. Assuming the elastic modulus and cross section do not vary over the length of the waveguide and uniform load, (B1) becomes

$$\frac{d^4}{dz^4}u(z) = \frac{p}{\mathcal{E}I}. \tag{B2}$$

Now, for our specific case, consider a situation where the beam, i.e., the waveguide, of length l, is fixed at both ends. This translates to boundary conditions $u(0) = 0$, $u(l) = 0$, $du/dz|_{z=0} = 0$, and $du/dz|_{z=l} = 0$. Applying these boundary conditions to (B2), we find

$$u(z) = \frac{p}{24\mathcal{E}I}(z^4 - 2lz^3 + l^2z^2). \tag{B3}$$

In our situation, $u(z)$ has an extremum at $z = l/2$, where the maximum deflection is

$$u_{\max} = u(l/2) = \frac{pl^4}{384\mathcal{E}I}. \tag{B4}$$

[1] J. W. Goodman, *Speckle Phenomena in Optics: Theory and Applications* (Roberts and Company, Greenwood Village, CO, 2007).

[2] K. Pearson, The problem of the random walk, Nature (London) **72**, 342 (1905).

[3] J.-H. Li, K. J. Webb, G. J. Burke, D. A. White, and C. A. Thompson, Design of near-field irregular diffractive optical elements by use of a multiresolution direct binary search method, Opt. Lett. **31**, 1181 (2006).

[4] M. Yang, H. Chen, K. J. Webb, S. Minin, S. L. Chuang, and G. R. Cueva, Demonstration of mode conversion in an irregular waveguide, Opt. Lett. **31**, 383 (2006).

[5] C. M. Bender and S. Boettcher, Real spectra in non-Hermitian Hamiltonians having $\mathcal{PT}$ symmetry, Phys. Rev. Lett. **80**, 5243 (1998).

[6] A. Ruschhaupt, F. Delgado, and J. Muga, Physical realization of $\mathcal{PT}$-symmetric potential scattering in a planar slab waveguide, J. Phys. A **38**, L171 (2005).

[7] A. Guo, G. J. Salamo, D. Duchesne, R. Morandotti, M. Volatier-Ravat, V. Aimez, G. A. Siviloglou, and D. N. Christodoulides, Observation of PT-symmetry breaking in complex optical potentials, Phys. Rev. Lett. **103**, 093902 (2009).

[8] P. Lebedew, Untersuchungen über die Druckkräfte des Lichtes, Ann. Phys. (Leipzig) **311**, 433 (1901).

[9] E. F. Nichols and G. F. Hull, The pressure due to radiation (second paper), Phys. Rev. (Series I) **17**, 26 (1903).

[10] P. W. Milonni and R. W. Boyd, Momentum of light in a dielectric medium, Adv. Opt. Photon. **2**, 519 (2010).

[11] K. J. Webb, Relationship between the Einstein-Laub electromagnetic force and the Lorentz force on free charge, Phys. Rev. B **94**, 064203 (2016).

[12] L.-F. Yang and K. J. Webb, Pushing and pulling optical pressure control with plasmonic surface waves, Phys. Rev. B **103**, 245124 (2021).

[13] K. J. Webb and Shivanand, Negative electromagnetic plane-wave force in gain media, Phys. Rev. E **84**, 057602 (2011).

[14] M. Mansuripur, A. R. Zakharian, and E. M. Wright, Electromagnetic-force distribution inside matter, Phys. Rev. A **88**, 023826 (2013).

[15] R. V. Jones and B. Leslie, The measurement of optical radiation pressure in dispersive media, Proc. R. Soc. London A **360**, 347 (1978).

[16] A. Ashkin and J. Dziedzic, Radiation pressure on a free liquid surface, Phys. Rev. Lett. **30**, 139 (1973).

[17] L.-F. Yang, A. Datta, Y.-C. Hsueh, X. Xu, and K. J. Webb, Demonstration of enhanced optical pressure on a structured surface, Phys. Rev. Lett. **122**, 083901 (2019).

[18] A. Ashkin, J. M. Dziedzic, J. E. Bjorkholm, and S. Chu, Observation of a single-beam gradient force optical trap for dielectric particles, Opt. Lett. **11**, 288 (1986).

[19] P. Polimeno, A. Magazzu, M. A. Iati, F. Patti, R. Saija, C. D. E. Boschi, M. G. Donato, P. G. Gucciardi, P. H. Jones, G. Volpe, and O. M. Marago, Optical tweezers and their applications, J. Quant. Spectrosc. Radiat. Transf. **218**, 131 (2018).

[20] M. Dienerowitz, M. Mazilu, and K. Dholakia, Optical manipulation of nanoparticles: a review, J. Nanophoton. **2**, 021875 (2008).

[21] F. Marquardt, A. Clerk, and S. Girvin, Quantum theory of optomechanical cooling, J. Mod. Opt. **55**, 3329 (2008).

[22] M. Aspelmeyer, T. J. Kippenberg, and F. Marquardt, Cavity optomechanics, Rev. Mod. Phys. **86**, 1391 (2014).

[23] B.-B. Li, L. Ou, Y. Lei, and Y.-C. Liu, Cavity optomechanical sensing, Nanophotonics **10**, 2799 (2021).

[24] L. K. Chin, Y. Shi, and A.-Q. Liu, Optical forces in silicon nanophotonics and optomechanical systems: Science and applications, Adv. Dev. Instrum. **2020**, 1964015 (2020).

[25] J. Ma and M. L. Povinelli, Effect of periodicity on optical forces between a one-dimensional periodic photonic crystal waveguide and an underlying substrate, Appl. Phys. Lett. **97**, 151102 (2010).

[26] J. Ma and M. L. Povinelli, Mechanical Kerr nonlinearities due to bipolar optical forces between deformable silicon waveguides, Opt. Express **19**, 10102 (2011).

[27] P. T. Rakich, P. Davids, and Z. Wang, Tailoring optical forces in waveguides through radiation pressure and electrostrictive forces, Opt. Express **18**, 14439 (2010).

[28] J. Roels, I. De Vlaminck, L. Lagae, B. Maes, D. Van Thourhout, and R. Baets, Tunable optical forces between nanophotonic waveguides, Nat. Nanotechnol. **4**, 510 (2009).

[29] M. L. Povinelli, S. G. Johnson, M. Lončar, M. Ibanescu, E. J. Smythe, F. Capasso, and J. Joannopoulos, High-Q enhancement of attractive and repulsive optical forces between coupled whispering-gallery-mode resonators, Opt. Express **13**, 8286 (2005).

[30] X. Yang, Y. Liu, R. F. Oulton, X. Yin, and X. Zhang, Optical forces in hybrid plasmonic waveguides, Nano Lett. **11**, 321 (2011).

[31] M. L. Povinelli, M. Lončar, M. Ibanescu, E. J. Smythe, S. G. Johnson, F. Capasso, and J. D. Joannopoulos, Evanescent-wave bonding between optical waveguides, Opt. Lett. **30**, 3042 (2005).

[32] A. Einstein and J. Laub, Über die im elektromagnetischen Felde auf ruhende Körper ausgeübten ponderomotorischen Kräfte, Ann. Phys. **331**, 541 (1908).

[33] K. J. Webb, Dependence of the radiation pressure on the background refractive index, Phys. Rev. Lett. **111**, 043602 (2013).

[34] I. Brevik, Experiments in phenomenological electrodynamics and the electromagnetic energy-momentum tensor, Phys. Rep. **52**, 133 (1979).

[35] S. M. Barnett and R. Loudon, On the electromagnetic force on a dielectric medium, J. Phys. B **39**, S671 (2006).

[36] B. Anghinoni, M. Partanen, and N. G. Astrath, The microscopic Ampère formulation for the electromagnetic force density in linear dielectrics, Eur. Phys. J. Plus **138**, 1034 (2023).

[37] K. J. Webb, Boundary condition for the optical force density, Phys. Rev. B **106**, 155423 (2022).

[38] A. W. Behnke, T. J. Pollei, and K. J. Webb, Einstein-Laub and Lorentz optical force densities with a planar interface, Phys. Rev. A **108**, 033708 (2023).

[39] F. I. Zahin, A. W. Behnke, T. J. Pollei, and K. J. Webb, Spatiotemporal force-density evolution in resonant structures with ultrafast optics, Phys. Rev. A **111**, 023514 (2025).

[40] J. D. Jackson, Poynting's theorem and conservation of energy and momentum for a system of charged particles and electromagnetic fields, in *Classical Electrodynamics*, 3rd ed. (Wiley, New York, 1999), Chap. 6.7, pp. 258.

[41] J. P. Gordon, Radiation forces and momenta in dielectric media, Phys. Rev. A **8**, 14 (1973).

[42] COMSOL Multiphysics® v. 6.2, www.comsol.com. COMSOL AB, Stockholm, Sweden.

[43] O. A. Bauchau and J. I. Craig, *Structural Analysis: With Applications to Aerospace Structures* (Springer Science & Business Media, Dordrecht, 2009), Vol. 163.

[44] A. Sánchez-Postigo, J. G. Wangüemert-Pérez, J. Soler Penadés, A. Ortega-Moñux, M. Nedeljkovic, R. Halir, F. El Mokhtari Mimun, Y. Xu Cheng, Z. Qu, A. Z. Khokhar, A. Osman, W. Cao, G. C. Littlejohns, P. Cheben, G. Z. Maschanovich, and Í. Molina-Fernández, Mid-infrared suspended waveguide platform and building blocks, IET. Optoelectron. **13**, 55 (2019).

[45] E. P. Tomasini and P. Castellini, *Laser Doppler Vibrometry* (Springer, Berlin, 2020).

[46] T. J. Pollei, A. W. Behnke, and K. J. Webb, Direct extraction of surface vibration profiles with optical beam deflection, Rev. Sci. Instrum. **97**, 025212 (2026).

[47] L. K. Sørensen, V. S. Gerasimov, S. V. Karpov, and H. Ågren, Development of discrete interaction models for ultrafine nanoparticle plasmonics, Phys. Chem. Chem. Phys. **26**, 24209 (2024).

[48] V. I. Zakomirnyi, Z. Rinkevicius, G. V. Baryshnikov, L. K. Sørensen, and H. Ågren, Extended discrete interaction model: plasmonic excitations of silver nanoparticles, J. Phys. Chem. C **123**, 28867 (2019).

[49] T. Feurer, N. S. Stoyanov, D. W. Ward, J. C. Vaughan, E. R. Statz, and K. A. Nelson, Terahertz polaritonics, Annu. Rev. Mater. Res. **37**, 317 (2007).

[50] K. J. Webb, L.-F. Yang, F. I. Zahin, and T. Intisar, Data: Optical force density in waveguides with broken symmetry, Purdue University Research Repository (PURR) (2026), https://doi.org/10.4231/WJ6N-7F27.